

Magnetic studies of 0.7(Fe₂O₃)/0.3(ZnO) nanocomposites in nanopowder form and dispersed in polymer matrix

JANUSZ TYPEK^{1*}, KAMIL WARDAL¹, GRZEGORZ ZOLNIERKIEWICZ¹, ANNA SZYMCZYK¹,
NIKOS GUSKOS^{1,2}, URSZULA NARKIEWICZ³, ELZBIETA PIESOWICZ⁴

¹Institute of Physics, West Pomeranian University of Technology, al. Piastow 48, 70-311 Szczecin, Poland

²Solid State Physics, Department of Physics, University of Athens, Panepistimiopolis, 15 784 Zografos, Athens, Greece

³Institute of Chemical and Environment Engineering, West Pomeranian University of Technology,
K. Pulaskiego10, 70-322 Szczecin, Poland

⁴Institute of Material Engineering, West Pomeranian University of Technology, al. Piastów 19, 70-310 Szczecin, Poland

Magnetic properties of 0.7(Fe₂O₃)/0.3(ZnO) nanocomposite synthesized by traditional wet chemistry method and containing only two phases: ZnO (nonmagnetic) and ZnFe₂O₄ (magnetic, with nanocrystallites of average size 12 nm, but forming large agglomerates, up to 100 nm in size) were studied by DC magnetization and ferromagnetic resonance (FMR). The investigated nanocomposite was either in a form of nanopowder or dispersed at concentration of 0.1 wt.% in poly(ethylene naphthalate-block-tetramethylene oxide) PTMO-b-PEN polymer matrix. Similarities and differences in magnetic behavior of these two samples revealed by the study of static magnetization and FMR spectra have been discussed relative to different morphologies and the associated variation of interparticle interactions. Moreover, thermal and thermo-oxidative stability of the nanocomposite and the neat polymer have been studied by thermogravimetric method.

Keywords: *ferromagnetic resonance; magnetization; thermogravimetry; zinc ferrite nanoparticles; polymer nanocomposite*

© Wrocław University of Technology.

1. Introduction

Nanocomposites with a general formula $n(\text{Fe}_2\text{O}_3)/(1-n)\text{ZnO}$, where the composition index $0 < n < 1$, have been intensively studied in the recent years [1]. They were synthesized by two methods: traditional wet chemical followed by calcination and the microwave assisted hydrothermal method. Scanning electron microscope images showed that samples obtained by the latter method were less agglomerated than the ones obtained by the former one. X-ray diffraction and Raman studies have shown that in the nanocomposites with the composition index $n \leq 0.70$ only two phases – ZnO and ZnFe₂O₄ – are present. In the nanocomposites with $n > 0.70$ the presence of yet another phase, $\gamma\text{-Fe}_2\text{O}_3$ (maghemite), has been detected and this phase is a dominating one in $n = 0.90$ and $n = 0.95$ samples.

The 0.7(Fe₂O₃)/0.3(ZnO) nanocomposite has been already the subject of a few recent papers [2–6]. The mean crystallite size of ZnFe₂O₄ was determined from Scherrer's formula and was equal to 12 nm. The morphology of the 0.7(Fe₂O₃)/0.3(ZnO) nanocomposite was investigated by using scanning electron microscopy (SEM) and spherical and elongated nanograins were observed. The observed peaks in low-frequency Raman spectra of ZnFe₂O₄ nanoparticles agree well with the calculated frequencies of acoustic phonons. The dynamic magnetic properties of 0.7(Fe₂O₃)/0.3(ZnO) nanocomposite studied by means of AC susceptibility at frequency of 625 Hz showed a typical behavior for a spin-glass system with the freezing temperature below 100 K.

Magnetic properties of ZnFe₂O₄ nanoparticles have been the subject of many studies because they are interesting and different than the ones registered in other ferrite spinels [7–12]. Bulk ZnFe₂O₄

*E-mail: typjan@zut.edu.pl

has a normal spinel structure, with the iron atoms located at octahedral B sites and Zn atoms occupying the tetrahedral A sites. Most iron-rich ferrites are ferrimagnetically ordered already at room temperature, but ZnFe₂O₄ is an antiferromagnet with the transition Neel temperature as small as $T_N = 10$ K. This difference is due to much weaker superexchange interaction between B sites than the corresponding A-B interaction. Therefore, a small migration of Fe atoms from B to A sites can produce ferrimagnetic regions with strong A-B superexchange interaction. This partial inversion is often made accountable for much higher T_N observed in ZnFe₂O₄ nanoparticles. It is still an open question whether that inversion takes place because of the chemical routes usually employed during the nanoparticle synthesis, or is it an intrinsic property of nanometric ZnFe₂O₄ particles caused by the finite-size effects.

The objective of this study is to compare magnetic properties of ZnFe₂O₄ nanoparticles in two forms: as a concentrated nanopowder and dispersed at very small concentration (0.1 wt.%) in non-magnetic matrix of PEN-b-PTMO polymer. For this aim DC magnetometry and ferromagnetic resonance (FMR) spectroscopy at microwave frequency have been employed. Moreover, the influence of the 0.7(Fe₂O₃)/0.3(ZnO) nanocomposite on thermal properties of PEN-b-PTMO polymer have been studied by thermogravimetric analysis (TGA).

2. Experimental

The 0.7(Fe₂O₃)/0.3(ZnO) nanopowder was synthesized by traditional wet chemistry method followed by calcination. A mixture of iron and zinc hydroxides was obtained by adding ammonia solution to the solution of proper amount of Zn(NO₃)₄·6H₂O and Fe(NO₃)₃·4H₂O in water. The obtained hydroxides were filtered, dried and calcined at 573 K during 1 hour. The details of synthesis were presented in the literature [5]. SEM and transmission electron microscopy (TEM) images of 0.7(Fe₂O₃)/0.3(ZnO) nanopowder are presented in Fig. 1. The SEM image shows strongly

agglomerated particles and the agglomerates are in size up to 100 nm, usually in the 30 nm to 60 nm range. The hexagonal crystals correspond to the ZnO, while the small spheroidal crystals to the ZnFe₂O₄ spinel. The TEM image shows a collection of nanocrystals whose sizes are roughly comparable to that what was determined by XRD. An average size of crystallites calculated from Scherrer's formula is obtained from XRD radiation diffracted on the whole sample, while TEM image shows only a very small part of that sample (selection problem), thus the former is more reliable. It is also known that nanoparticles sizes determined by TEM and XRD can differ because in general the nanoparticles are non-spherical and have an inhomogeneous sizes distribution [13].

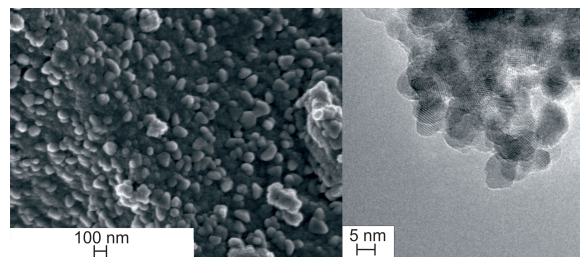


Fig. 1. SEM (left) and TEM (right) images of 0.7(Fe₂O₃)/0.3(ZnO) nanopowder.

The poly(ethylene naphthalate-block-tetramethylene oxide) (PEN-b-PTMO) copolymer containing 0.7(Fe₂O₃)/0.3(ZnO) nanopowder as nanofiller was prepared by melt polycondensation of dimethyl 2,6-naphthalenedicarboxylate (DMN, Fluca), ethylene glycol (EG, Sigma-Aldrich), and poly(tetramethylene ether) glycol (PTMEG with molecular weight of 1000 g/mol, terathane 1000 DuPont) in the presence of zinc acetate and antimony oxide as catalysts and phenolic antioxidant IRGANOX 1010 (Ciba-Geigy) as stabilizers. In the first step the nanopowder in the ethylene glycol was grinded and stirred. In the second step the obtained dispersion was sonicated. These two processes were repeated to ensure a stable distribution of the nanopowder in the glycol matrix. Subsequently, all substrates were introduced into the reactor, where the two-stage process of multiblock poly(ether-ester)

copolymer (PEN-b-PTMO) synthesis proceeded with continuous mixing. The first stage of the multiblock process was the transesterification of DMN with EG in the presence of catalyst (zinc oxide, 0.25 wt.% in relation to DMN) which was carried out under atmospheric pressure in 150 °C to 190 °C temperature range. The progress of that reaction was measured by the amount of methanol distilled in the reaction. In the second stage, the polycondensation of diol-ether (PTMG) with bis(2-hydroxyethylene) naphthalate was carried out in the presence of tetrabutyl orthotitanate as a catalyst at 280 °C and under pressure of 10 Pa. The viscosity of the reaction mixture increased in the condensation polymerization as the reaction progressed what was monitored by observing the stirring torque. The nanocomposite and neat PTT-b-PTMO copolymer syntheses were finished when the melt reached the same value of viscosity at 280 °C. The molten copolymer was extruded from the autoclave into the water cooled bath.

FMR measurements in the 4 K to 290 K range were performed on a conventional magnetic resonance spectrometer Bruker E 500 with 100 kHz magnetic field modulation using an Oxford helium-flow cryostat. FMR measurements in the 290 K to 423 K range were done on a Radiopan SE/X 2544-M spectrometer equipped with a homemade high-temperature unit. DC magnetization study in the 6 K to 300 K range was performed using Quantum Design Magnetic Property Measurements System MPMS XL-7 with a superconducting quantum interference device magnetometer. Thermogravimetric measurements were carried out on SETARAM TGA 92-16 apparatus in the temperature range from 10 °C to 700 °C under dynamic atmosphere of argon and air (the flow rate was 20 cm³/min), at the heating rate of 10 °C/min.

3. Results and discussion

3.1. DC magnetometry

In Fig. 2 temperature dependence of the DC magnetic susceptibility χ (defined as $\chi = M/H$) in zero field cooled (ZFC) and field cooled (FC) modes of the 0.7(Fe₂O₃)/0.3(ZnO) nanopowder (Fig. 2a) and the 0.7(Fe₂O₃)/0.3(ZnO) dispersed in

polymer (Fig. 2b) measured in two different magnetic fields ($H = 100$ Oe and 1000 Oe) is presented. In ZFC mode all magnetic moments in each single domain particle point along the nanoparticle easy axis when the nanoparticles are cooled down to very low temperature and magnetic anisotropy prevents switching of magnetization from the easy axis. As a result, the average magnetization is very small at low temperature because of random distribution of the easy axis directions. The magnetic anisotropy in some nanoparticles is overcome and the magnetization directions of these thermally activated nanoparticles start to align with the applied field as the temperature is increased and, as a result, the total magnetization initially increases with increasing temperature, reaching a maximum at the corresponding temperature T_{\max} . For non-interacting particles this temperature is directly proportional to the average blocking temperature T_B . In case of our nanopowder sample $T_{\max} = 81$ K and 36 K in magnetic field $H = 100$ Oe and 1000 Oe, respectively. For 0.7(Fe₂O₃)/0.3(ZnO) dispersed in polymer $T_{\max} = 70$ K and 34 K in magnetic field $H = 100$ Oe and 1000 Oe, respectively. These temperatures are slightly lower in polymer sample indicating weaker anisotropy due to reduced magnetic interaction and probably smaller sizes of ZnFe₂O₄ nanoparticles.

Interestingly, very similar results concerning the field dependence of T_{\max} in concentrated and diluted samples of iron oxide nanoparticles were obtained by Knobel *et al.* [14]. They found that in low magnetic fields T_{\max} is higher for the concentrated sample than for the diluted one and that this difference in T_{\max} vanishes in higher magnetic fields. This is exactly the same phenomenon as was observed in our samples. Yet another interesting effect of interparticle dipolar interaction was seen in the temperature dependence of FC magnetization below T_{\max} [14]. While the FC curve of the diluted sample was kept increasing as T was decreasing below T_{\max} , the FC of the concentrated sample remained almost constant. A similar effect can be found in FC magnetization in our samples (Fig. 2).

In FC mode of magnetization study all the magnetic moments of the nanoparticles are aligned

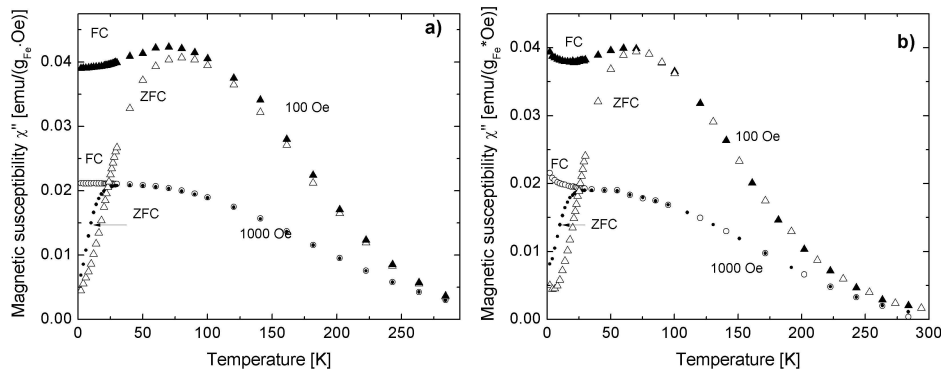


Fig. 2. Temperature dependence of the magnetic susceptibility in ZFC and FC modes of 0.7(Fe₂O₃)/0.3(ZnO) nanopowder (a) and dispersed in polymer 0.7(Fe₂O₃)/0.3(ZnO) (b) measured in two different magnetic fields (100 Oe and 1000 Oe).

along the external field direction, irrespective of the easy axis orientation of each individual nanoparticle and at low temperature the magnetization direction of each particle is frozen in the field direction. During temperature rise an increasing number of nanoparticles will be in a superparamagnetic state and the magnetization should decrease monotonically. Such behavior is observed in our samples for sufficiently large external magnetic fields ($H \sim 1$ kOe), but for weaker fields non-monotonic $M_{FC}(T)$ dependence is observed, especially for the nanopowder sample. This may be the result of magnetic interparticle interactions.

As can be observed in Fig. 2 the ZFC and FC curves diverge below a certain temperature T_{irr} called irreversibility temperature, where a magnetic irreversibility is observed. This temperature can be related to the blocking temperature of the largest in size particles. Therefore the difference between T_{irr} and T_{max} can be taken as the particle size distribution (in the absence of interparticle interactions). Closer inspection of Fig. 2 shows that T_{irr} strongly depends on external magnetic field H . For the nanopowder sample in $H = 100$ Oe $T_{irr} \approx 200$ K, while in $H = 1000$ Oe the irreversibility temperature is very close to T_{max} . In case of the polymer sample, both temperatures are similar, $T_{irr} \approx T_{max}$ independent of external magnetic field. That dissimilar behavior of both investigated samples in the context of magnetic irreversibility could be attributed to non-negligible interparticle interaction in the nanopowder sample.

In Fig. 3 isothermal magnetization of nanopowder and polymer samples in magnetic field up to 70 kOe is presented. For the nanopowder sample (Fig. 3a) no saturation even in the strongest available field was reached. At temperature higher than the blocking temperature, in the superparamagnetic phase, magnetization $M(H)$ is expected to follow the Langevin, $M = M_S \cdot L(x)$, or modified Langevin function, $M = M_S \cdot L(x) + \alpha H$, where $L(x) = \coth(x) - \frac{1}{x}$ is the Langevin function and $x = \frac{\mu_p H}{kT}$. Here, M_S is the saturation magnetization, μ_p is the particle magnetic moment, k is the Boltzmann constant and α is linear susceptibility. For isothermal magnetization of nanopowder sample at $T = 290$ K it was found that the modified Langevin function is better than the classical Langevin in fitting experimental points, although even that fit is not quite satisfactory. One of the reasons might be a broad distribution of particle sizes and particle magnetic moments in 0.7(Fe₂O₃)/0.3(ZnO) nanopowder [15]. The effective magnetic moment of one Fe³⁺ ion calculated from the obtained value of M_S was only 0.5 Bohr magnetons what is well below for an expected value for spin-only magnetism of iron ion and thus it might be the evidence of the core-shell structure of investigated nanoparticles.

Isothermal magnetization of the polymer sample (Fig. 3c and Fig. 3d) is fairly different from the nanopowder sample. Due to a small concentration of ferromagnetic nanoparticles, the diamagnetic properties of the PEN-b-PTMO polymer matrix

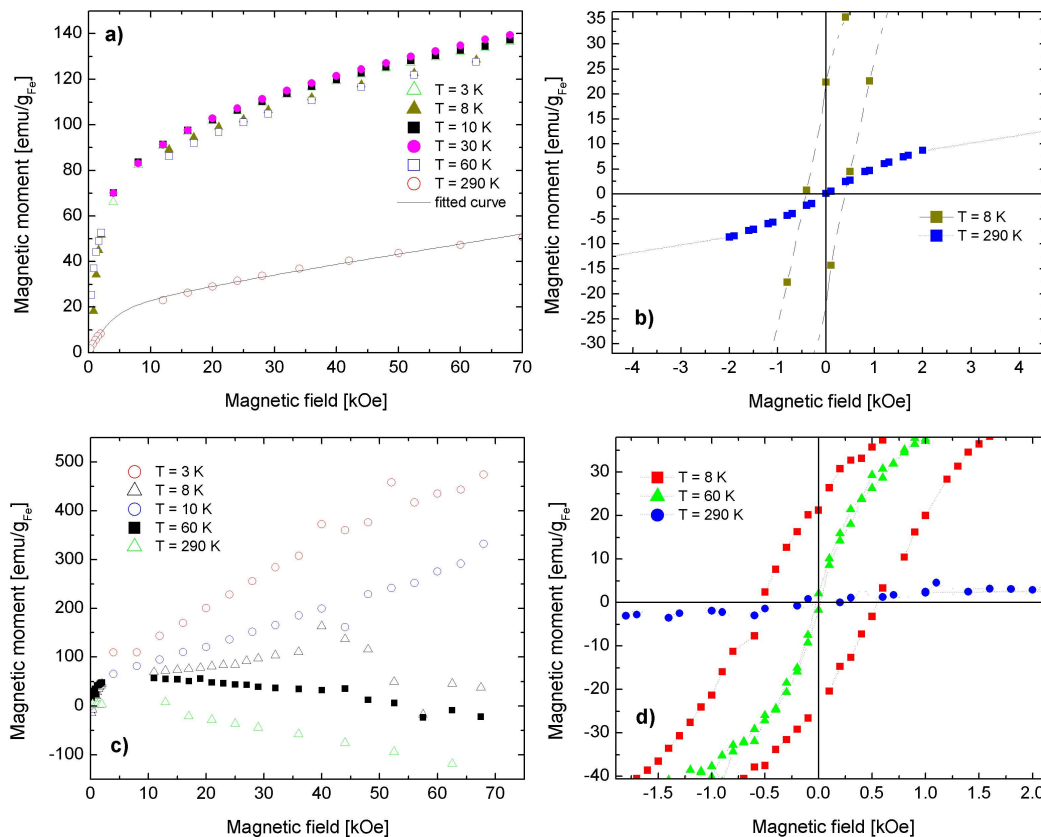


Fig. 3. Isothermal magnetization $M(H)$ of nanopowder sample (a, b) and polymer sample (c, d). Solid line in (a) for $T = 290$ K is the fit to the modified Langevin function. (b) and (d) present magnetization in low magnetic fields (hysteresis loops).

prevail in strong magnetic fields and at higher temperatures so the resulting magnetization becomes negative. Fig. 3b and Fig. 3d present magnetization in small magnetic fields (hysteresis loops) for a nanopowder and polymer sample, respectively. At temperature $T = 8$ K, well below T_{\max} , in weak magnetic fields, the hysteresis loop in $M(H)$ magnetization is observed for both samples (Fig. 3b and Fig. 3d). For the nanopowder sample the coercive field is 390 Oe, while for the polymer sample it is 480 Oe. Also the remanent magnetization is slightly bigger for the polymer sample than for the nanopowder one, 23 emu/g_{Fe} and 20 emu/g_{Fe} , respectively. For the nanopowder sample the hysteresis loop is only observed at the lowest temperatures ($T < 10$ K) indicating the existence of ferromagnetic state in that temperature range. Bearing in mind the $M(T)$ curve for the nanopowder sample it could be deduced that the spin-glass state is

formed at higher temperatures, up to T_{\max} , depending strongly on applied magnetic field. Above T_{\max} the superparamagnetic phase is expected.

Matrix effects on magnetic properties of $\gamma\text{-Fe}_2\text{O}_3$ (maghemite) nanoparticles dispersed in a multiblock copolymer have been investigated previously [16]. Behavior of two polymer samples with magnetic nanoparticles in two different dispersion forms (large agglomerates and separate nanoparticles) was compared. It was found that the shift of T_{\max} in $M_{\text{ZFC}}(T)$ curves towards higher temperatures as well as the broadening of the $M_{\text{ZFC}}(T)$ peak and flattening of the $M_{\text{ZFC/FC}}(T)$ curves above T_{\max} is the sign of an increased interaction between nanoparticles. Exactly the same behavior was seen in our $0.7(\text{Fe}_2\text{O}_3)/0.3(\text{ZnO})$ nanopowder sample in which strong interparticle interactions have been expected.

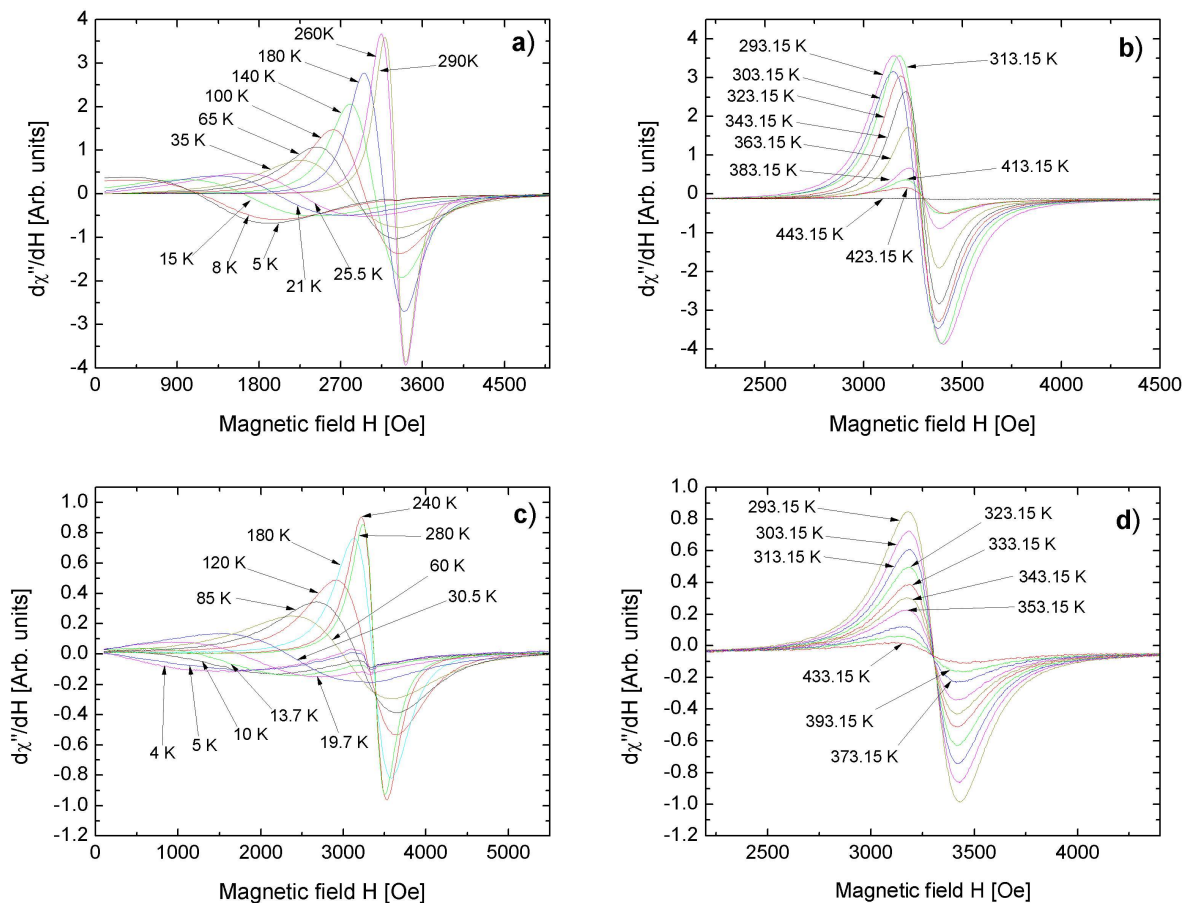


Fig. 4. FMR spectra of 0.7(Fe₂O₃)/0.3(ZnO) nanopowder (a, b) and dispersed in polymer 0.7(Fe₂O₃)/0.3(ZnO) (c, d) recorded at a few different temperatures.

The magnetization $M(H)$ of large aggregates was smaller than that of separate nanoparticles and exhibited a relatively slower increment at low fields in the study of maghemite samples [16]. This was also confirmed in our study of 0.7(Fe₂O₃)/0.3(ZnO) nanopowder and polymer samples. As the hysteresis loop is concerned the coercive field was bigger for the sample containing agglomerated maghemite nanoparticles than for the dispersed ones [16]. In case of our 0.7(Fe₂O₃)/0.3(ZnO) samples a reversed effect was registered: the coercive field was bigger for the polymer sample. While a significant decrease of both coercivity and remanence has been predicted for interacting single domain particles with dipolar forces, a more complex behavior may arise from the interplay of exchange interactions and magnetic anisotropy [17]. In case for our polymer

sample the bigger coercive field could be attributed to interaction of ZnFe₂O₄ nanoparticles with the polymer matrix.

3.2. Ferromagnetic resonance

FMR spectra of nanopowder and nanopowder dispersed in PEN-b-PTMO polymer taken at different temperatures in the 4 K to 423 K range are presented in Fig. 4. In Fig. 4a and Fig. 4b FMR spectra of nanopowder in low and high temperature ranges are shown, respectively. Similarly, in Fig. 4c and Fig. 4d the spectra of 0.7(Fe₂O₃)/0.3(ZnO) nanocomposite dispersed in polymer matrix are displayed. Above room temperature (RT) a single, nearly symmetrical and narrow line is registered that decreases in intensity with temperature

increase in both samples. On cooling the samples from RT the amplitude of the resonance line decreases, the apparent resonance field decreases, the apparent linewidth increases and the lineshape becomes visibly asymmetrical (the apparent parameters are measured directly from the observed spectra). Such behavior is typical of FMR spectra of magnetic nanoparticles in the superparamagnetic phase [12, 18]. The values of apparent resonance fields (Fig. 5, right axis) and linewidths are similar for both types of the samples.

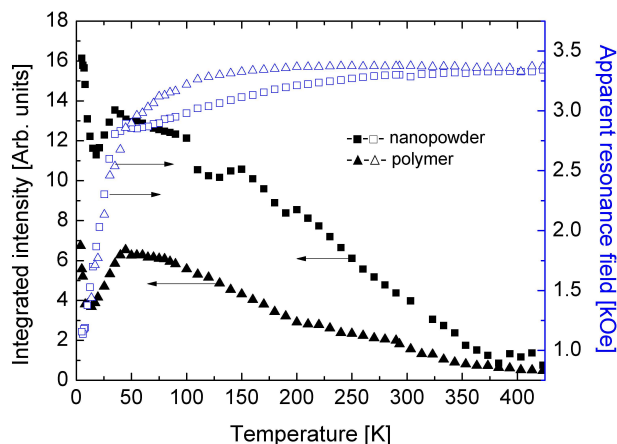


Fig. 5. Integrated intensity (left axis) of nanopowder (full squares) and polymer (full triangles) samples, and apparent resonance field (right axis) of nanopowder (open squares) and polymer (open triangles) samples.

Closer inspection of the temperature dependence of the apparent resonance fields (Fig. 5, right axis) reveals that in the case of polymer sample it increases slightly on cooling from RT down to about 150 K but decreases on further cooling, especially strongly below 50 K. The apparent resonance field is slightly smaller in the nanopowder sample what can be explained by the existence of bigger internal field in that stronger magnetic material. The shift of the resonance field toward lower magnetic field could be explained by the core-shell model [19]. The core is assumed to be in the ferromagnetic (superparamagnetic) state and the surface layer in the paramagnetic state. The non-uniform surface magnetization produces unidirectional field seen by the bulk spins which causes

temperature-dependent shift of the FMR line towards lower fields. Strong surface anisotropy results in an increase of the average resonance frequency of the surface spins. Due to exchange interactions, this frequency shift is partly transferred to the bulk spin system, leading to the corresponding shift of the FMR spectrum toward lower fields [19].

Fig. 5 (left axis) presents also the temperature dependence of the integrated intensity. The integrated intensity, calculated as an area under the absorption curve (not the first derivative shown in Fig. 4), is proportional to the magnetic susceptibility of the spin system at a microwave frequency. As seen in Fig. 5 it behaves similarly in both samples. It increases with temperature decrease from RT and reaches a maximum at about 45 K in the polymer sample (35 K in the nanopowder sample) followed by a strong decrease down to 12 K in the polymer sample (18 K in the nanopowder sample). Below that minimum in the integrated intensity, it starts to increase again with temperature decrease. As can be easily noticed the temperature difference between the maximum and minimum in integrated intensity is much narrower in the nanopowder sample and is shifted towards lower temperatures. It might be connected with stronger magnetic interactions in that sample. The observed maximum in the temperature dependence of the integrated intensity curve is often identified with the so called blocking temperature below which most of nanoparticles have fixed in space magnetic moment that could not be reversed by thermal motion. Another, more plausible explanation is related to an effective anisotropy field of a nanoparticle becoming larger at that temperature than the characteristic microwave field of the spectrometer [20, 21]. A steep increase of the integrated intensity with decreasing temperature at the lowest temperatures (below 19 K and 12 K for the nanopowder and polymer samples, respectively) can be attributed to the existence of a spurious paramagnetic phase or paramagnetic component in the core-shell model of ZnFe_2O_4 nanoparticles [18].

All the registered FMR spectra could be very well fitted with the sum of two Landau-Lifshitz

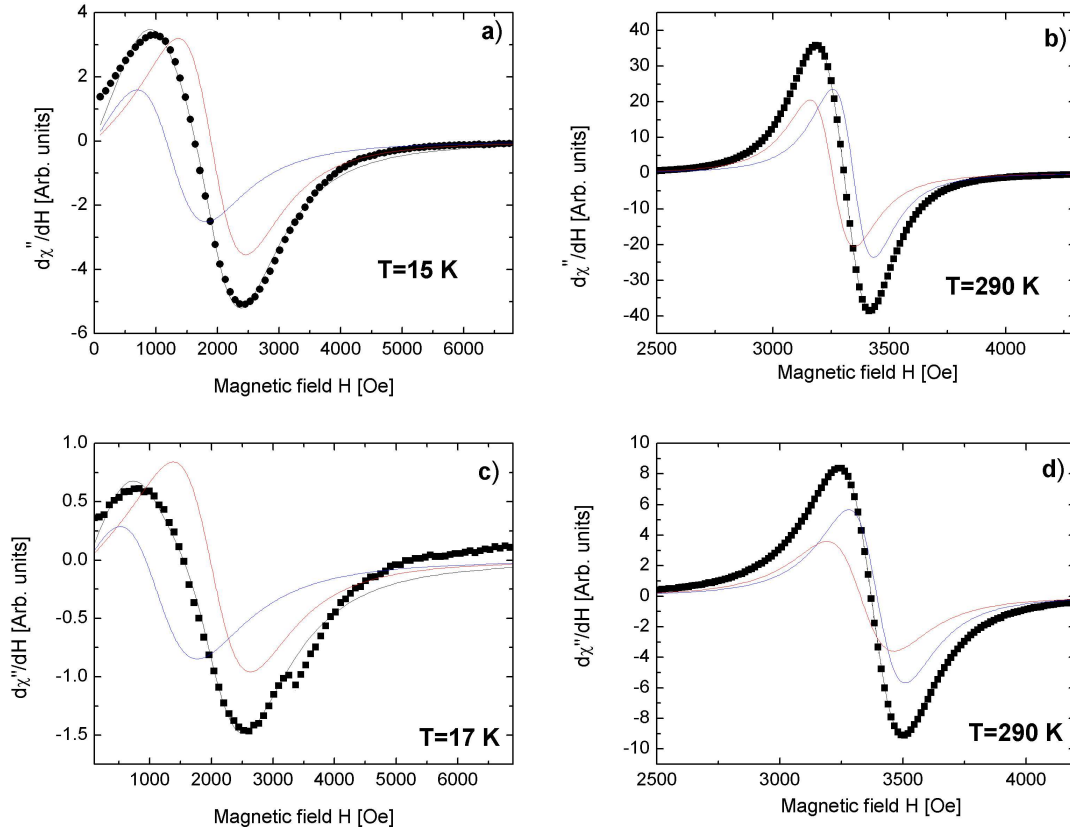


Fig. 6. Experimental (dots) and fitted (line) FMR spectra, with two components of fitted line of 0.7(Fe₂O₃)/0.3(ZnO) nanocomposite at 15 K (a), 290 K (b) and the nanocomposite doped in the polymer PEN-b-PTMO at 17 K (c), 290 K (d).

(LL) lines (Fig. 6). The LL lineshape function is given by the following equation:

$$\chi''(H) = \frac{1}{\pi} \frac{H_r^2 [(H_r^2 + \Delta_H^2)H^2 + H_r^4] \Delta_H}{[H_r^2 (H - H_r)^2 + H^2 \Delta_H^2] [H_r^2 (H + H_r)^2 + H^2 \Delta_H^2]} \quad (1)$$

where H_r is the true resonance field and Δ_H is the true linewidth. Usage of the two LL components can be explained by assuming two anisotropy axes of a nanoparticle which are arranged perpendicularly to each other. Because each registered FMR spectrum is produced by an array of many individual nanoparticles with the anisotropy axes randomly oriented in respect to an external magnetic field, the decomposition of FMR spectrum on only two component lines is just a fairly coarse approximation. However, it could provide an estimation of the value of magnetic anisotropy in the nanoparticles system. Each registered spectrum was fitted

with two LL lines that corresponded to two orientations – parallel and perpendicular – of an external magnetic field with respect to the effective nanoparticle anisotropy axis. In Fig. 6, as an example, the experimental and fitted spectra taken at low and high temperatures in both types of samples are presented. Additionally, each component is also drawn. It is easily to notice that the experimental spectrum could be very well fitted with only these two components.

Temperature dependence of the true resonance fields H_r and true linewidths Δ_H calculated from equation 1 for two LL components and for two investigated samples is presented in Fig. 7 and Fig. 8. The linewidths of two components in each sample increase with cooling down the samples from RT. This is typical of FMR spectra of magnetic nanoparticles. The broadening is especially strong

in the low temperature range, below ~ 40 K (Fig. 8) and is correlated with a rapid decrease of the resonance field. This sudden broadening might be interpreted in terms of the spin-glass freezing of the particle surface layer. This effect seems to be stronger in polymer sample, probably due to interaction with the surrounding matrix, as evidenced by broader linewidths registered at the lowest temperature.

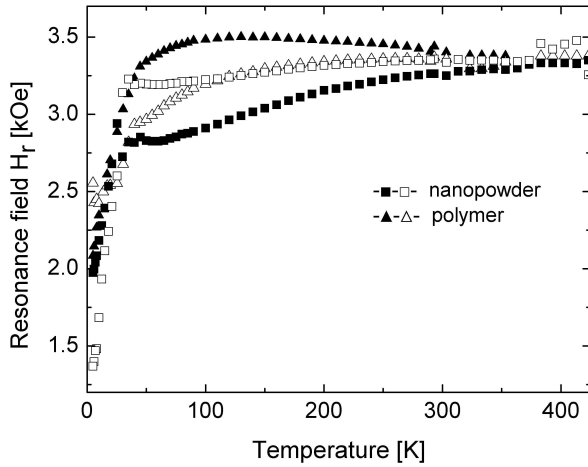


Fig. 7. Temperature dependence of the calculated true resonance field of the nanopowder (full and open squares) and the polymer (full and open triangles) samples.

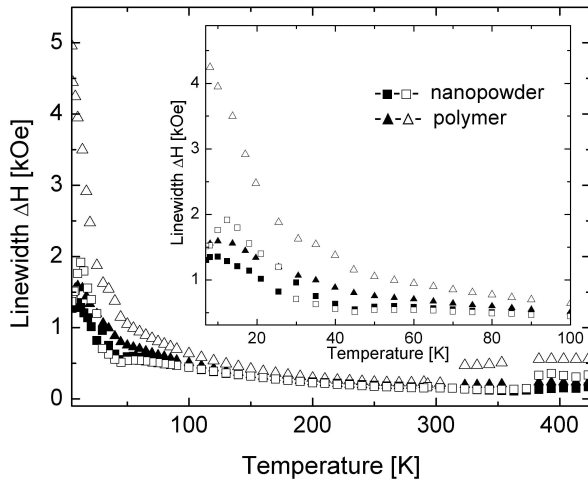


Fig. 8. Temperature dependence of the calculated true linewidth of the nanopowder (full and open squares) and the polymer (full and open triangles) samples.

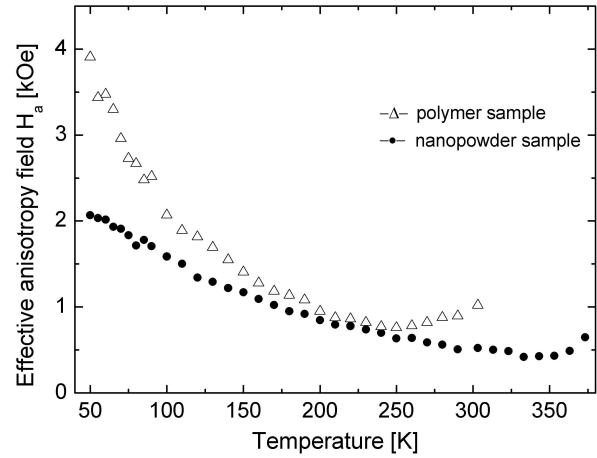


Fig. 9. Temperature dependence of the effective anisotropy field H_a calculated from equation 3 for both types of samples.

According to the procedure presented in the literature [21], the difference of the resonance fields of both components in each sample can be correlated with the effective anisotropy field H_a of that sample [22]. As the linewidths of the two components are not very small, the relaxation effects influencing the resonance fields must be taken into account. If H_r is the observed resonance field with relaxation effects and H_r^0 is the resonance field without relaxation, the following relation holds:

$$H_r^0 = H_r + \frac{3\Delta H_{pp}^2}{4H_r} \quad (2)$$

where ΔH_{pp} is the observed peak-to-peak linewidth. The effective uniaxial anisotropy field H_a could be calculated from the resonance fields of both LL components without relaxation as [23]:

$$H_a = \frac{2}{3} (H_{r1}^0 - H_{r2}^0) \quad (3)$$

The obtained from equation 3 H_a values as a function of temperature are presented in Fig. 9. In general, the anisotropy field is slightly stronger in the polymer sample and increases with temperature decrease (for $T < 250$ K and $T < 350$ K for the polymer and nanopowder samples, respectively) for both studied samples. It is also evident that temperature change of the anisotropy field is more accentuated in the polymer sample and that points

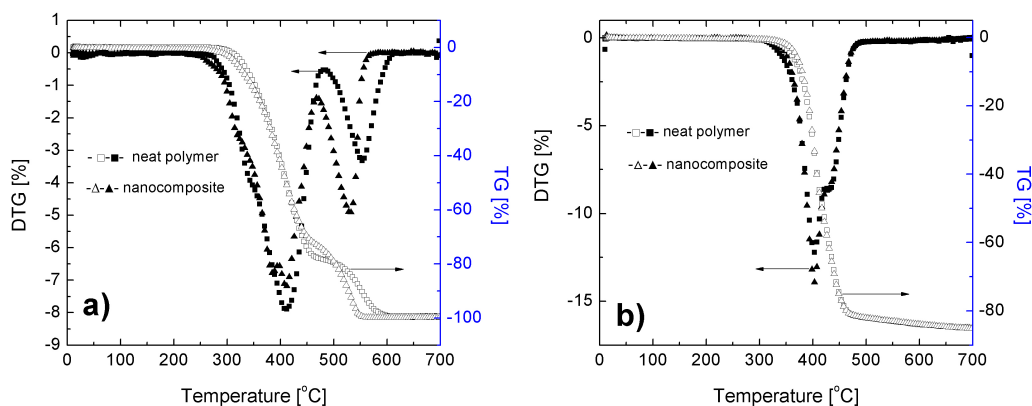


Fig. 10. Heat flow of neat PEN-b-PTMO (full squares) and PEN-b-PTMO containing 0.1 % of the nanopowder (full triangles), mass loss of neat PEN-b-PTMO (open squares) and PEN-b-PTMO containing 0.1 % of the nanopowder (open triangles), in air (a) and in argon (b) atmosphere.

to a stronger contribution of the surface anisotropy in that sample caused probably by the surrounding matrix. Similar results were obtained in the investigation of magnetite (Fe₃O₄) nanoparticles with different sizes [23].

3.3. Thermal and thermo-oxidative stability

PTMO-based poly(ether-esters) copolymers are sensitive to oxidative degradation due to the ether soft block. It is well known that the mechanism of the thermo-oxidative degradation of these copolymers involves a radical chain process with formation of hydroperoxides at the carbon adjacent to the ether oxygen [24]. The effect of the presence of 0.7(Fe₂O₃)/0.3(ZnO) in PTT-PTMO matrix on thermal and oxidative stability of the composite was studied by thermogravimetric analysis (TGA). The mass loss (TG) and the DTG (derivative of TG) curves for the nanocomposite and the neat copolymer (without nanofiller) under oxidative (air) and inert (argon) atmosphere are presented in Fig. 10. From the shape of the TG and DTG curves for the nanocomposite and the neat PEN-b-PTMO copolymer, it can be observed that in air and in an inert atmosphere (argon) the thermal behavior of the composite and neat copolymer is very similar. The PEN-PTMO copolymer in oxidative atmosphere has two stages of degradation,

which appear in 250 °C to 450 °C and 450 °C to 600 °C ranges. The first step of decomposition is attributed to the decomposition of flexible polyether and rigid polyester segments and the second step is ascribed to the decomposition of the residue [25]. The temperatures at the maximum decomposition rate (maximum on DTG peak) of the main decomposition step in air (at 405 °C) and in argon (at 400 °C) are not induced by the presence of the nanofiller in the copolymer matrix. In air, the first stage of decomposition is slightly influenced by the presence of the nanofiller. The value of temperature corresponding to the 10 % weight loss is shifted to lower temperatures. This indicates that the nanocomposite has lower thermo-oxidative stability than the neat PEN-b-PTMO copolymer. This can be explained by the catalysing of the decomposition reaction by the presence of metal oxide or the increasing of molecular weight polydispersity of the block copolymer in the composite which results in higher concentration of the functional groups (OH, COOH).

4. Conclusions

Static magnetization and FMR measurements of two samples: 0.7(Fe₂O₃)/0.3(ZnO) nanopowder and that nanofiller in PEN-b-PTMO copolymer have revealed similarities and differences in their magnetic response that reflect specific constitution

of nanoparticle agglomerates and their interaction with each other and with their environment. As the morphology of the ZnFe_2O_4 nanoparticles agglomerates in both types of samples is concerned, the magnetic measurements indicate that the agglomerates are smaller in the polymer sample (T_{max} is lower in the polymer sample) and their sizes distribution is also narrower ($T_{\text{irr}} \approx T_{\text{max}}$) than in the nanopowder sample. On broad distribution of sizes in nanopowder sample indicates also $M(H)$ curve in that sample. As the dipolar inter-particle interaction is concerned it is stronger in nanopowder sample and that is evidenced by the shape of $M_{\text{FC}}(T)$ curve and by thermal dependence of FMR spectra. On the other hand, in polymer sample there are stronger interactions of agglomerates with their environment (polymer chains in case of polymer sample and neighbouring agglomerates in nanopowder sample). This is confirmed by bigger coercive field H_c , broader FMR line and bigger anisotropy field H_a in that sample. Moreover, nanofiller in the polymer sample shifts to lower temperature the first stage of its decomposition.

References

- [1] TYPEK J., WARDAL K., ZOLNIERKIEWICZ G., GUSKOS N., NARKIEWICZ U., *Magnetic Properties of $\text{Fe}_2\text{O}_3/\text{ZnO}$ Nanocomposites*, in: BONCA J., KRUCHININ S. (Eds.), *NATO Science for Peace and Security Series C: Environmental Security, Nanotechnology in the Security Systems*, Springer, Dordrecht, 2015, p. 93.
- [2] GUSKOS N., ZOLNIERKIEWICZ G., TYPEK J., SIBERA D., NARKIEWICZ U., *Rev. Adv. Mater. Sci.*, 23 (2010), 224.
- [3] GUSKOS N., TYPEK J., ZOLNIERKIEWICZ G., WARDAL K., SIBERA D., NARKIEWICZ U., *Rev. Adv. Mater. Sci.*, 29 (2011), 142.
- [4] KURLISZ-KUDELSKA I., HADZIC B., SIBERA D., ROMCEVIC M., ROMCEVIC N., NARKIEWICZ U., DOBROWOLSKI W., *J. Alloy. Compd.*, 509 (2011), 3756.
- [5] NARKIEWICZ U., SIBERA D., KURLISZYN-KUDELSKA I., KILANSKI L., DOBROWOLSKI W., ROMCEVIC N., *Acta Phys. Pol. A*, 113 (2008), 1695.
- [6] KURLISZYN-KUDELSKA I., DOBROWOLSKI W., ARCISZEWSKA M., ROMCEVIC N., ROMCEVIC M., HADZIC B., SIBERA D., NARKIEWICZ U., LOKOWSKI W., *Sci. Sinter.*, 45 (2013), 31.
- [7] SINGH D.J., GUPTA M., GUPTA R., *Phys. Rev. B*, 63 (2001), 205102.
- [8] BOHRA M., PRASAD S., KUMAR N., MISRA D.S., SAHOO S.C., VENKATARAMANI N., KRISHNAN R., *Appl. Phys. Lett.*, 88 (2006), 26206.
- [9] KARMAKAR D., MANDAL S.K., KADAM R.M., PAULOSE P.L., RAJARAJAN A.K., NATH T.K., DAS A.K., DASGUPTA I., DAS G.P., *Phys. Rev. B*, 75 (2007), 144404.
- [10] BLANCO-GUTIERREZ V., SAEZ-PUCHE R., TORRALVO-FERNANDEZ M., *J. Mater. Chem.*, 22 (2012), 2992.
- [11] KOSEGLU Y., YILDIZ H., YILGIN R., *J. Nanosci. Nanotechnol.*, 12 (2012), 2261.
- [12] WARDAL K., TYPEK J., ZOLNIERKIEWICZ G., GUSKOS N., NARKIEWICZ U., SIBERA D., *Eur. Phys. J. Appl. Phys.*, 62 (2013), 10402.
- [13] BORCHERT H., SHEVCHENKO E.V., ROBERT A., MEKIS I., KORNOWSKI A., GRUBEL G., WELLER H., *Langmuir*, 21 (2005), 1931.
- [14] KNOBEL M., NUNES W.C., WINNISCHOFER H., ROCHA T.C.R., SOCOLOVSKY L.M., MAYORGA C.L., ZANCHET D., *J. Non-Cryst. Solids*, 353 (2007), 743.
- [15] TIWARI S.D., RAJEEV K.P., *Solid State Commun.*, 152 (2012), 1080.
- [16] GUSKOS N., GLENIS S., LIKODIMOS V., TYPEK J., MARYNIAK M., ROSLANIEC Z., KWIATKOWSKA M., BARAN M., SZYMCZAK R., PETRIDIS D., *J. Appl. Phys.*, 99 (2006), 084307.
- [17] CHANTRELL R.W., WALMSLEY N.S., GORE J., MAYLIN M., *Phys. Rev. B*, 63 (2000), 024410.
- [18] TYPEK J., WARDAL K., GUSKOS N., SIBERA D., NARKIEWICZ U., *IEEE T. Magn.*, 50 (2014), 6101606.
- [19] NOGINOVA N., CHEN F., WEAVER T., GIANNELIS E.P., BOURLINOS A.B., ATSARKIN V.A., *J. Phys., Condens. Matter*, 19 (2007), 246208.
- [20] BIASI DE E., ZYSLER R.D., RAMOS C.A., ROMERO H., *J. Magn. Magn. Mater.*, 294 (2005), e87.
- [21] BIASI DE E., LIMA JR. E., RAMOS C.A., BUTERA A., ZYSLER R.D., *J. Magn. Magn. Mater.*, 326 (2013), 138.
- [22] ZINS D., NAKATSUKA K., GENDRON F., RIVOIRE M., *J. Magn. Magn. Mater.*, 201 (1999), 84.
- [23] VARGAS J.M., LIMA JR. E., ZYSLER R.D., DUQUE J.G.S., DE BIASI E., KNOBEL M., *Eur. Phys. J. B*, 64 (2008), 211.
- [24] SZYMCZYK A., ROSLANIEC Z., *Polimery-W.*, 51 (2006), 627.
- [25] SZYMCZYK A., *J. Appl. Polym. Sci.*, 126 (2012), 796.

Received 2015-05-20
Accepted 2016-01-11